Error Performance of MPSK Trellis-Coded Modulation over Nonindependent Rician Fading Channels

C. Tellambura and Vijay K. Bhargava, *Fellow, IEEE*

***Abstract*—This paper presents new upper bounds on the pairwise error probability (PEP) of trellis-coded modulation (TCM) schemes over *nonindependent* Rician fading channels. Cases considered are coherent and pilot-tone-aided detection and differential detection of trellis-coded multilevel phase-shift keying (TC-MPSK) systems. The average bit-error probability P_b can be approximated by truncating the union bound. This method does not necessarily lead to an upper bound on P_b, and, hence, the approximation must be used with simulation results. In addition, for Rayleigh fading channels with an exponential autocovariance function, bounds resembling those for memoryless channels have been derived. The bounds are substantially more accurate than Chernoff bounds and hence allow for accurate estimation of system performance when the assumption of ideal interleaving is relaxed.**

***Index Terms*—Interleaving, Rician fading, trellis coding.**

I. Introduction

THE USE of trellis-coded modulation (TCM) for these mobile communication channels, typically modeled as Rician or Rayleigh, has recently received wide attention. Interleaving is a commonly used technique to break up burst errors caused by amplitude fades. The duration of the fades, an indication of the channel memory, depends on the Doppler spread of the fading process. Given a block interleaver of size $N_d \times N_s$, as result of interleaving/deinterleaving, the fading process experienced by the receiver varies N_d times faster than that of a noninterleaved case, i.e., the effective channel memory is reduced by a factor of $1/N_d$. Accordingly, a channel is said to be *ideally interleaved* if $N_d \to \infty$ and *nonideally interleaved* if N_d is finite (correlated fading).

Thus, it is clear that the channel memory is reduced, but not eliminated with nonideal interleaving. In this work, the effect of this residual memory on the average bit error probability P_b of TCM is addressed. In particular, consideration is given to how large N_d should be in order that P_b approaches that of ideal interleaving. To compute the union bound on P_b, one needs formulas for the pairwise error probability (PEP), the probability that the decoder selects the erroneous codeword when given only two choices. To compute the PEP of TCM schemes in fading channels, the probability that a quadratic decision variable (i.e., the difference between the two path metrics, assuming Viterbi decoding, of the two codewords) in complex normal variables is less than a certain threshold must be calculated. In general, this probability cannot be obtained analytically, although the characteristic function of the decision variable is known in closed form.

An early paper [1] presents an analysis of a maximal-ratio combiner for nonindependent fading among the signals. The sum of the received powers is a positive-definite quadratic form, and the characteristic function method provides the density function of the sum. Because of the duality between diversity methods and coding, for instance, for binary convolutional codes the PEP can be obtained similarly [2].

The performance of coding schemes in correlated fading channels has been examined mostly through computer simulation, but [2]–[8] provide both analytical and simulation results. References [2]–[6] deal with convolution codes, while [7] and [8] with trellis-coded modulation in correlated Rayleigh fading. Direct extension of the results in [2] to the TCM case may not be fruitful because the Chernoff bound is known to be weak when applied to TCM schemes [9].

For TCM over Rayleigh fading channels, the PEP can be expressed in terms of the eigenvalues of a weighted covariance matrix. In [7] and [9], a method to compute the exact PEP for this case has been given; it involves evaluating residues. P_b is estimated by computing exact PEP's for a set of dominant error events. However, for Rician channels, computation of the exact PEP is possible only via numerical integration.

In this paper, we present two new upper bounds on the PEP for a correlated Rician fading channel. The method requires computing eigenvalues, but avoids integration, and is significantly more accurate than a Chernoff bound for this case. The bounds are derived assuming the pilot-tone concept, and hence can be modified to several useful cases including ideal coherent detection, coherent detection based on a pilot-tone, and differential detection. The average bit-error probability P_b can be approximated by truncating the union bound to include a finite set of dominant (short) error events. This method, however, does not always lead to an upper bound on P_b, because when the correlation increases, the PEP's of long error events do not decay rapidly and the tail of the union bound may not even converge. Hence, the approximation must be used cautiously and with relevant simulation results. For

Manuscript received March 26, 1993; revised August 4, 1995. This work was supported by a Strategic Research Grant awarded by the Natural Sciences and Engineering Council of Canada (NSERC).

C. Tellambura is with the Department of Digital Systems, Monash University, Clayton, Victoria 3168, Australia.

V. K. Bhargava is with the Department of Electrical and Computer Engineering, University of Victoria, Victoria, B.C., Canada V8W 3P6.

Publisher Item Identifier S 0018-9545(98)00713-0.

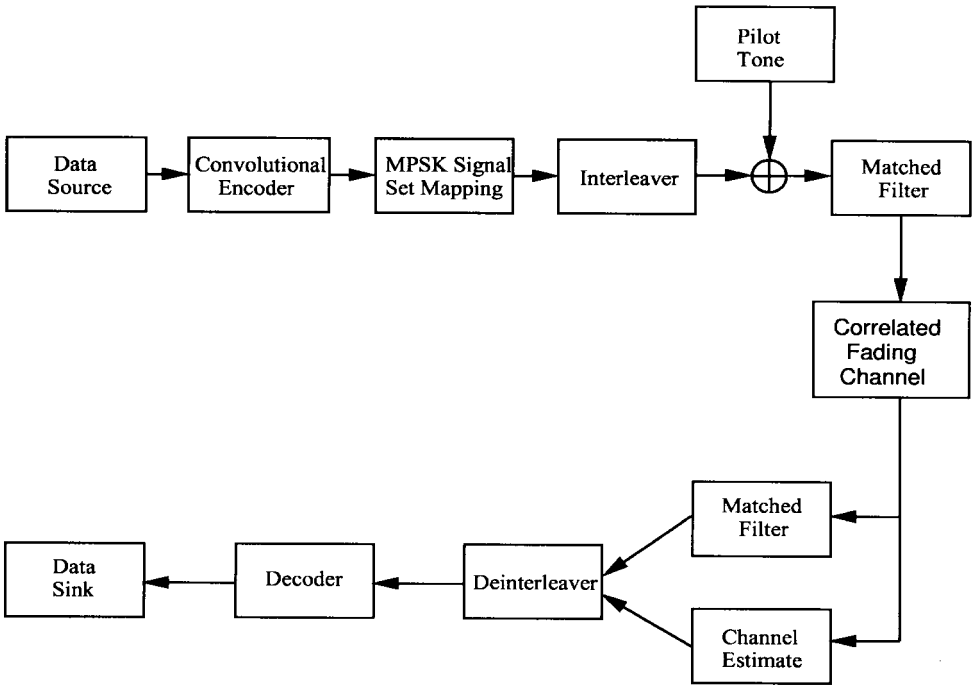

Fig. 1. Baseband system model.

a Rayleigh fading channel with exponential correlation, by assuming the worst codeword to be the one in which all error symbols are consecutive, the PEP bound can be simplified to a form resembling that of memoryless channels. Thus, P_b can be bounded using the transfer function technique, based on the method of Zehavi and Wolf [10]. Comparisons with simulation results show that the estimates of P_b are quite accurate when the interleaving depth N_d is sufficiently large.

The paper is organized as follows. Section II describes the system model used here and the characterization of Rician fading channels. The bounds are derived in Sections III and IV. Several examples are presented in Section V. Finally, conclusions are provided in Section VI.

II. System Description

The system under consideration, as described in [11] and [12], is shown in Fig. 1. Binary input data is convolutionally encoded at rate $n/(n+1)$, where n is the number of information bits per encoding interval. The encoded $n+1$ bit words are block interleaved and mapped into a sequence $\boldsymbol{x} = (x_1, x_2, \cdots, x_N)$ of M-ary PSK symbols, which constitute a normalized constellation, meaning that

$$x_i \in \{\exp(j2\pi k/M) : k = 0, 1, \cdots, M-1\}$$

for all symbols. The receiver deinterleaves and then applies soft-decision Viterbi decoding. A block interleaver of N_s columns (interleaving span) and N_d (interleaving depth) rows of memory is considered here.

The transmitted signal in the baseband is [9]

$$c(t) = \sum_{k=-\infty}^{\infty} v_k s(t - kT_s) \tag{1}$$

where $s(t)$ is a unit-energy pulse that satisfies Nyquist's conditions for zero intersymbol interference, T_s is the symbol duration, and

$$v_k = \begin{cases} x_k & \text{TC-MPSK} \\ v_{k-1}x_k & \text{TC-MDPSK} \end{cases} \tag{2}$$

where x_k denotes the kth convolutional encoder output. Here, the acronym TC-MDPSK denotes trellis-coded M-ary differential phase-shift keying. The transmitted sequence, because of interleaving, will be a scrambled version of the encoder output sequence; to simplify notation, this rearrangement is not explicitly shown in (1). Instead, the effect of interleaving is accounted for by increasing the effective Doppler rate.

The signal is demodulated using a filter matched to $s(t)$. Hence, the received sample corresponding to the kth coded symbol can be denoted by

$$y_k = \alpha_k v_k + n_k \tag{3}$$

where n_k is a complex-Gaussian random variable with zero mean and variance $\sigma^2 = (2\gamma_s)^{-1}$, where $\gamma_s = \overline{E}_s/N_0$. Here, $\overline{E}_s/N_0$ denotes the average signal energy-to-noise spectral density ratio. The channel gain α_k is complex Gaussian with the averages

$$\langle \alpha_k \rangle = A \qquad \frac{1}{2}\langle (\alpha_k - A)(\alpha_k - A)^* \rangle = b_0 \tag{4}$$

where the constant mean A denotes the line-of-sight (LOS) and specular components of the received signal, and b_0 is the variance of the diffuse component (Rayleigh fading) of the received signal. The normalizations $A^2 + 2b_0 = 1$ and $K = A^2/2b_0$ enable the Rician channel to be characterized by a single parameter K. For Rayleigh fading, $A = 0$ and $b_0 = 0.5$. Note that in (3) the fading process, although fluctuating from one symbol interval to the next, remains

constant over the duration of a symbol [piecewise constant (PC)]. The PC approximation holds for a Doppler rate less than 5% of the symbol rate (i.e., $f_D T_s \leq 0.05$). For a baud rate 2400 symbols/s, this corresponds to a Doppler rate of 120 Hz, which is a worst case rate for current mobile communication systems. Reference [13] discusses the validity of this model. Also, in [4] and [5] the authors evaluate the performance of coded binary PSK in Rician fading channels, with or without the PC approximation.

Clearly, the set of the α_k's forms a PC approximation to the continuous random process $\alpha(t)$, and this approximation converts, in effect, $\alpha(t)$ into a process with a discrete time parameter. Recognizing that the α_k in (3) have been deinterleaved, which increases the time separation between, say, α_{k_1} and α_{k_2} in (3) to $N_d T_s|k_1 - k_2|$ instead of $T_s|k_1 - k_2|$ (for nointerleaving), two possible models for the normalized autocovariance function of this discrete channel are

$$\rho(k_1 - k_2) = \begin{cases} J_0(2\pi f_D N_d T_s|k_1 - k_2|) & k_1, k_2 \in \{0, 1, 2, \cdots\} \\ \exp(-2\pi f_D N_d T_s|k_1 - k_2|) \triangleq q^{|k_1 - k_2|} \end{cases} \quad (5)$$

where f_D is the Doppler spread of the fading process, N_d is the interleaving depth, and $J_0(\cdot)$ is the zero-order Bessel function. Alternatively, (5) can be interpreted as indicating that the effective fade rate at the decoder is $N_d f_D$. In the above, the Bessel autocovariance corresponds to the land-mobile spectrum, while the exponential corresponds to the first-order Butterworth spectrum. Other possible correlation models are given in [12].

Equation (5) may not be true in some cases, and hence its validity must be qualified as follows. Consider a set of N channel gains in (3) $(\alpha_1, \cdots, \alpha_N)$ corresponding to a transmitted codeword of the same length. The above time separation relation holds only if all components of the transmitted codeword had been confined to a single row of the transmitter buffer. Fortunately, for most dominant error events, $N \ll N_s$, and hence we assume that this condition is true. This phenomenon has been described in detail in [7] for the block interleaver.

III. Pairwise Error Probability

In the following, we derive an upper bound on the PEP when nonideal interleaving exists. The upper bound is quite general in that it is derived for the pilot-tone concept [9], [14], which encompasses cases such as ideal and partial coherent detection, differential detection, etc.

According to the pilot-tone concept, an estimate $\hat{\alpha}_k$ of the true channel gain α_k is obtained by processing samples of the pilot-tone, which is transmitted along with the data. In order to evaluate the error performance, a statistical description of $\hat{\alpha}_k$ is necessary. Namely, $\hat{\alpha}_k$ is Gaussian with mean $\langle \hat{\alpha}_k \rangle$ and variance

$$b_1 = \frac{1}{2}\langle (\hat{\alpha}_k - \langle \hat{\alpha}_k \rangle)(\hat{\alpha}_k - \langle \hat{\alpha}_k \rangle)^* \rangle.$$

The normalized correlation coefficient between α_k and $\hat{\alpha}_k$ is

$$\mu = \frac{1}{2}\langle (\alpha_k - \langle \alpha_k \rangle)(\hat{\alpha}_k - \langle \hat{\alpha}_k \rangle)^* \rangle / \sqrt{b_0 b_1}.$$

Following [9], we take the Viterbi decoder metric to be Euclidean, that is

$$m(y_k, x_k) = -|y_k - \hat{\alpha}_k x_k|^2. \quad (6)$$

Note that decoding with this decoding metric is not necessarily optimum for nonideally interleaved channels. The optimum decoder metric would presumably take into account the residual correlations [14, Ch. 11]. However, for ease of analysis and implementation, this metric is used.

The PEP $P(\boldsymbol{x} \to \hat{\boldsymbol{x}})$ is defined to be the probability of choosing the coded sequence $\hat{\boldsymbol{x}} = (\hat{x}_1, \hat{x}_2, \cdots, \hat{x}_N)$ when $\boldsymbol{x} = (x_1, x_2, \cdots, x_N)$ was transmitted. Let $\eta \triangleq \{k : x_k \neq \hat{x}_k\}$ and let L denote the number of elements in η, which is known as the "length" of the error event. The smallest possible L, L_{min}, is known as the code *diversity*. Also, $S = \max(\eta) - \min(\eta) + 1$ is called the "span" of the error event [7]. Obviously, if $L = S$, then the L elements of η are contiguous; that is, $\eta = \{k_0, k_0 + 1, \cdots, k_0 + L - 1\}$ for some k_0. Unlike for binary convolutional codes, this condition holds for most error events in typical TCM schemes.

The PEP, by using the fact that the total metric for a codeword is the sum of component metrics, is

$$P(\boldsymbol{x} \to \hat{\boldsymbol{x}}) = \Pr\{\Xi \geq 0\}$$

where

$$\Xi = \sum_{k \in \eta} y_k \hat{\alpha}_k^* (\hat{x}_k - x_k)^* + y_k^* \hat{\alpha}_k (\hat{x}_k - x_k). \quad (7)$$

Let V_k denote the 2×1 column matrix $V_k = (\hat{\alpha}_k \;\; y_k)^T$. The decision variable Ξ can then be represented as

$$\Xi = \sum_{k \in \eta} V_k^\dagger F_k V_k = \boldsymbol{V}^\dagger \boldsymbol{F} \boldsymbol{V} \quad (8)$$

where the dagger denotes conjugate transpose, $\boldsymbol{V} = (V_1, V_2, \cdots, V_L)^T$, and $\boldsymbol{F}$ is a diagonal matrix with diagonal entries being

$$F_k = \begin{pmatrix} 0 & (\hat{x}_k - x_k)^* \\ (\hat{x}_k - x_k) & 0 \end{pmatrix}. \quad (9)$$

From (3) and (4), it follows that each V_k is Gaussian with the mean $\langle V \rangle = (A, Ax_k)^T$ and the 2×2 covariance matrix

$$R_k = \begin{pmatrix} b_1 & \mu\sqrt{b_0 b_1} x_k \\ \mu^* \sqrt{b_0 b_1} x_k^* & b_0 + \sigma^2 \end{pmatrix}. \quad (10)$$

We also need the covariance matrix $\boldsymbol{R}$ of the random vector $\boldsymbol{V}$, and $\boldsymbol{R}$ is defined as

$$\boldsymbol{R} = \frac{1}{2}\langle [\boldsymbol{V} - \langle \boldsymbol{V} \rangle]^* [\boldsymbol{V} - \langle \boldsymbol{V} \rangle]^T \rangle. \quad (11)$$

For ideally interleaved channels, this matrix will be tridiagonal, consisting only of R_k terms as defined by (10). To see how $\boldsymbol{R}$ is obtained for nonideal interleaving, consider the case of ideal coherent detection. Thus, the channel estimates $\hat{\alpha}_k = \alpha_k$, their variance $b_1 = b_0$, and the correlation coefficient $\mu = 1$. Assuming, without loss of generality, that the all-zero symbol sequence is transmitted, R_k can be readily obtained. To find the

remaining elements of $\boldsymbol{R}$, we note that $V_i = (\alpha_i, y_i)^T$ and that the covariance between V_i and V_j $(i \neq j,\ i,j = 1,2,\cdots,L)$ is

$$\frac{1}{2}\langle (V_i - \langle V_i\rangle)(V_j - \langle V_j\rangle)^T\rangle = b_0\begin{pmatrix}\rho(|i-j|) & \rho(|i-j|)\\ \rho(|i-j|) & \rho(|i-j|)\end{pmatrix}. \tag{12}$$

A similar approach can be taken for differential detection and pilot-tone-aided detection [15].

A. The PEP

To upper-bound the PEP, we introduce the following lemma, which is a slight modification of a lemma derived in [3, Appendix 2].

Lemma 1: Let U be a random variable, $w_U(x)$ its probability density function (pdf), and $\phi_U(\omega) \triangleq \overline{\exp(j\omega U)}$ its characteristic function. Then

$$\Pr[U \geq 0] < \frac{1}{2\pi}\int_{-\infty}^{\infty} \frac{|\phi_U(\alpha - j\beta)|}{\sqrt{\alpha^2+\beta^2}}\, d\alpha, \qquad \beta_0 > \beta > 0 \tag{13}$$

where β_0 is the boundary of the convergence region of the integral

$$\int_{-\infty}^{\infty} w_U(x)\exp(\beta x)\, dx.$$

Proof: From [3]

$$\Pr[U \geq 0] = \frac{1}{2\pi}\int_{-\infty}^{\infty} \frac{\phi_U(\alpha - j\beta)}{\beta - j\alpha}\, d\alpha, \qquad \beta_0 > \beta > 0. \tag{14}$$

Since

$$\left|\int g\, d\alpha\right| \leq \int |g|\, d\alpha$$

the lemma follows immediately. When using this lemma, one needs to know the value of β_0, which, as will be seen next, depends on the largest positive eigenvalue of $\boldsymbol{R^*F}$. For ideally interleaved channels, β_0 can be found easily.

Now, the characteristic function of Ξ (7) is given by [14, Appendix B]

$$G_\Xi(\xi) = \prod_{k=1}^{2L} \frac{1}{1-2j\xi\phi_k}\exp\left[\frac{j\xi\phi_k|\langle\eta_k\rangle|^2}{1-2j\xi\phi_k}\right] \tag{15}$$

where ϕ_k, $k = 1,2,\cdots,2L$ are the eigenvalues of $\boldsymbol{R^*F}$. Note that $\boldsymbol{R^*}$ has positive eigenvalues, but due to the structure of $\boldsymbol{F}$ the matrix $\boldsymbol{R^*F}$ has L positive eigenvalues and L negative ones. Thus, let $\phi_k < 0$ for $k = 1,2,\cdots,L$ and $\phi_k > 0$ for $k = L+1,\cdots,2L$. To obtain this form of the characteristic function, the set of random variables V_k must be transformed to another set of $2L$ independent variables, where the transformation simultaneously diagonalizes both $\boldsymbol{R}$ and $\boldsymbol{F}$. The η_k's are the means of these transformed variables. Details of this transformation are given in [14, Appendix B].

To apply (13) to bound the PEP, one needs the range of β, which is related to the positive poles of $G_\Xi(\xi)$. Since β must be less than the minimum pole on the right-hand plane, the range of β is

$$0 < \beta < \left[\frac{1}{2\phi_{\max}}\right] \tag{16}$$

where $\phi_{\max}$ denotes the largest positive eigenvalue, i.e., $\max(\phi_k|\ k = L+1,\cdots,2L)$. Having established the range of β, we combine (13) and (15) to obtain

$$P(\boldsymbol{x}\to\hat{\boldsymbol{x}}) < \frac{1}{2\pi}\int_{-\infty}^{\infty}\frac{1}{\sqrt{\alpha^2+\beta^2}}\prod_{k=1}^{2L}\frac{\exp(v_k)}{|1-2j\beta\phi_k - 2j\alpha\phi_k|}\, d\alpha \tag{17}$$

where

$$v_k = \mathrm{Real}\left(\frac{(\beta+j\alpha)\phi_k|\langle\eta_k\rangle|^2}{1-2\beta\phi_k-2j\alpha\phi_k}\right). \tag{18}$$

By multiplying the numerator and the denominator of this with the conjugate of the denominator and selecting the real part of the resulting expression, it can readily be shown that

$$v_k \leq \frac{\beta\phi_k|\langle\eta_k\rangle|^2}{1-2\beta\phi_k}. \tag{19}$$

Thus, we have

$$P(\boldsymbol{x}\to\hat{\boldsymbol{x}}) < \frac{1}{2\pi}\int_{-\infty}^{\infty}\frac{1}{\sqrt{\alpha^2+\beta^2}}\prod_{k=1}^{2L}\frac{\exp\left(\frac{\beta\phi_k|\langle\eta_k\rangle|^2}{1-2\beta\phi_k}\right)}{|1-2\beta\phi_k-2j\alpha\phi_k|}\, d\alpha. \tag{20}$$

In principle, we need to find the β, which minimizes this upper bound, a quite difficult task. Instead, we may choose

$$\beta = \frac{1}{2}\left[\frac{1}{2\phi_{\max}}\right] \tag{21}$$

and evaluate (20) numerically, which again is computationally intensive. Dividing each square root in the product by $4\phi_k^2$, (20) can be recast as

$$P(\boldsymbol{x}\to\hat{\boldsymbol{x}}) < \Lambda(\beta)\frac{\exp[\beta\langle V\rangle^\dagger(\boldsymbol{F^{-1}}-2\beta\boldsymbol{R^*})^{-1}\langle V\rangle]}{|\det(2\,\boldsymbol{R^*F}\,)|} \tag{22}$$

where $|\bullet|$ denotes the absolute value

$$\Lambda(\beta) \triangleq \frac{1}{2\pi}\int_{-\infty}^{\infty}\prod_{k=0}^{2L}\frac{1}{\sqrt{(\alpha^2+\beta_k^2)}}\, d\alpha \tag{23}$$

and where $\beta_0 = \beta$, $\beta_k = |(1/2\phi_k - \beta)|$ for $k = 1,2,\cdots,2L$. Since all other terms in (22) can be readily computed, it remains to compute $\Lambda(\beta)$, and this is made difficult by the fact that the integrand contains square roots. Fortunately, this difficulty can be circumvented by using Schwarz's inequality. Define

$$\psi_1(\alpha) \triangleq \prod_{k=0}^{L}\frac{1}{\sqrt{\alpha^2+\beta_k^2}}, \qquad \psi_2(\alpha) \triangleq \prod_{k=L+1}^{2L}\frac{1}{\sqrt{\alpha^2+\beta_k^2}}. \tag{24}$$

Schwarz's inequality yields the following:

$$\Lambda(\beta) \leq \frac{1}{2\pi}\left(\int_{-\infty}^{\infty}\psi_1^2(\alpha)\, d\alpha\int_{-\infty}^{\infty}\psi_2^2(\alpha)\, d\alpha\right)^{1/2}. \tag{25}$$

Now, each integral can be evaluated by considering the complex integral $\oint f(z)\,dz$ in a semicircular-shaped contour. The details of this technique can be found in many textbooks on complex analysis. Thus $\Delta_{ik} = (\beta_i^2 - \beta_k^2)$

$$\Lambda(\beta) < \frac{1}{2}\left(\sum_{k=0}^{L}\frac{1}{\beta_k}\prod_{\substack{i=0\\ i\neq k}}^{L}\frac{1}{\Delta_{ik}}\right)^{1/2}\left(\sum_{k=L+1}^{2L}\frac{1}{\beta_k}\prod_{\substack{i=L+1\\ i\neq k}}^{2L}\frac{1}{\Delta_{ik}}\right)^{1/2}. \tag{26}$$

In deriving this, it is tacitly assumed that the β_k's $(k = 1, 2, \cdots, 2L)$ are distinct. This is indeed the case for nonideal interleaving. However, depending on the structure of the error event, with ideal interleaving, there may exist repeated eigenvalues. In this case (26) must be modified accordingly.

Combining (22) and (26), we get

$$P(\boldsymbol{x} \to \hat{\boldsymbol{x}}) < \tilde{\Lambda}(\beta)\frac{\exp\left[\beta\langle V\rangle^{\dagger}(\boldsymbol{F}^{-1} - 2\beta\boldsymbol{R}^{*})^{-1}\langle V\rangle\right]}{|\det(2\boldsymbol{R}^{*}\boldsymbol{F})|} \tag{27}$$

where $\tilde{\Lambda}(\beta)$ is the upper bound on $\Lambda(\beta)$, as defined by (26). It will be shown later that this upper bound is extremely accurate and remains so even when no interleaving is employed. Furthermore, little is to be gained by searching for the β that minimizes this bound, and for this reason the choice (21) will be adequate.

Note that this bound can be readily used with a union bound to get an upper bound of the bit-error probability

$$P_b \le \frac{1}{n}\sum_{j=1}^{\infty} w(j) P_j(\boldsymbol{x} \to \hat{\boldsymbol{x}}) \tag{28}$$

where $w(j)$ is the number of bit errors associated with the jth error event, and n is the number of information bits per encoding interval. Obviously, in order to limit computations, this summation must be terminated after a finite number of error events, assuming that the remainder is negligible. As observed in [2], for sufficiently large γ_s and $N_d f_D T_s$, the union bound is dominated by a small set of error events. However, for low values of γ_s and $N_d f_D T_s$, the union bound itself becomes loose [2].

B. Simplified Error Bound

Since computing (27) requires all the eigenvalues $(2L)$, simplifying it is desirable. The difficulty stems from the fact that the β_k's are distinct. This suggests the possibility of replacing the β_k's with β_0 in (23), which holds only if $\beta_k^2 \le \beta_0^2$ for $\forall k$ (otherwise, (22) is no longer an upper bound). For the choice $\beta = 1/4\phi_{\max}$, $1 - 4\beta\phi_{\max} \ge 0, \forall k$, which implies that

$$\left(\frac{1}{2\phi_{\max}} - \beta\right)^2 \ge \beta^2$$

the desired condition. Inserting this in (23) and combining with (22) gives

$$P(\boldsymbol{x} \to \hat{\boldsymbol{x}}) < \Lambda_1(\beta)\frac{\exp\left[\beta\langle V\rangle^{\dagger}(\boldsymbol{F}^{-1} - 2\beta\boldsymbol{R}^{*})^{-1}\langle V\rangle\right]}{|\det(2\boldsymbol{R}^{*}\boldsymbol{F})|} \tag{29}$$

where

$$\Lambda_1(\beta) = \frac{1}{2\pi}\int_{-\infty}^{\infty}\frac{1}{(\alpha^2 + \beta^2)^{L+1/2}}\,d\alpha \tag{30}$$

which can be evaluated in terms of the gamma function. Using an identity involving the gamma function [16, (5.2)], the integral evaluates to

$$\Lambda_1(\beta) = \frac{1}{2\pi\beta^{2L}}\frac{\Gamma(1/2)\Gamma(L)}{\Gamma(L+1/2)} \tag{31}$$

where

$$\Gamma(n) = \int_0^{\infty} e^{-x}x^{n-1}\,dx \tag{32}$$

converges for all $n > 0$. Combining (29) and (31), we get

$$P(\boldsymbol{x} \to \hat{\boldsymbol{x}}) < \frac{B(L)\exp\left[\beta\langle V\rangle^{\dagger}(\boldsymbol{F}^{-1} - 2\beta\boldsymbol{R}^{*})^{-1}\langle V\rangle\right]}{(4\phi_{\max})^{-2L}|\det(2\boldsymbol{R}^{*}\boldsymbol{F})|} \tag{33}$$

where

$$B(L) \triangleq \frac{1}{2\pi}\frac{\Gamma(1/2)\Gamma(L)}{\Gamma(L+1/2)}. \tag{34}$$

While simpler than (27), this bound is substantially weaker for limited interleaving with slow fading. The reason is that in deriving this bound, the terms $1 - 2\beta\phi_k$ in the denominator of (20) have been neglected [cf. (23) and (30)].

IV. Rayleigh Fading Channels

We would like to further simplify (33) to a product form that can be used in conjunction with the transfer function technique, as is the case in independent fading channels. This may not be done for Rician fading since the exponential term in (33) may not factor into a suitable product form. For Rayleigh fading channels, however, the exponential term in (33) is zero, and this enables us to reduce the other terms to a product form. For this purpose, we select an exponential autocovariance function [see (5)] since this function leads to expressions, as will be seen later, that are factorable, which may not be possible for other covariance models. Also, in the following we assume that for any error event, say, between $\boldsymbol{x}$ and $\hat{\boldsymbol{x}}$, the elements in error are adjacent (i.e., $x_k \neq \hat{x}_k$ for $k = k_0, \cdots, k_0 + L - 1$ given the length to be L). While this may not hold for some error events, it allows for a simple error bound because it enables the simplification of the determinant of $\boldsymbol{R}$ needed in (33). Since in an exponentially correlated channel the correlation between any two channel gains monotonically increases as the time separation between the two decreases, this assumption leads to a pessimistic error bound. A similar approach in the case of convolutional codes over correlated Rician fading channels is considered in [2] and [4].

If the maximum eigenvalue $\phi_{\max}$ can be bounded by a number that is independent of the structure of an error event, then (33) can be further simplified. This is possible for ideal interleaving, as the eigenvalues of $\boldsymbol{R}^{*}\boldsymbol{F}$ can be determined by considering each 2×2 matrix product $\boldsymbol{R}_k^{*}\boldsymbol{F}_k$. Let ϕ_{k-} and ϕ_{k+} denote these two eigenvalues. Assuming μ to be real and

using (9) and (10), it can be readily proven that all positive ϕ_{k+} satisfy the inequality

$$\phi_{k+} < \frac{((1-\mu^2)b_0+\sigma^2)}{\mu\sqrt{b_0/b_1}}. \tag{35}$$

It is conjectured that this bound on the $\phi_{\max}$ also holds for the case of nonideal interleaving. In other words, it is conjectured that the largest positive eigenvalue of $\boldsymbol{R}^*\boldsymbol{F}$ does not increase above the value given in (35) when the normalized correlation between adjacent channel gains q changes from $q = 0$ to $q > 0$. This can be proven for error events of length two (see Appendix I). In fact, all entries that contain q will be off the main diagonal of $\boldsymbol{R}^*\boldsymbol{F}$, which suggests that for small q values the eigenvalues change very little. We have observed this numerically. Thus, from (21), the choice of β is

$$\beta = \frac{\mu\sqrt{b_0/b_1}}{4((1-\mu^2)b_0+\sigma^2)}. \tag{36}$$

Clearly, the eigenvalue bound (35) and hence (36) will be most accurate when the interleaving capacity is nearly ideal, otherwise, (for slow fading and low or no interleaving capacity, $q \approx 1$) it will be substantially weaker. This behavior will be considered later.

To further simplify (33), we also need the determinant of $\boldsymbol{R}$, given in Appendix II. Combining (29), (36), and (A.10), we get

$$P(\boldsymbol{x} \to \hat{\boldsymbol{x}}) < \tilde{B}(L) \prod_{k=1}^{L} \frac{1}{4\beta^2\Upsilon|x_k - \hat{x}_k|^2} \tag{37}$$

where

$$\tilde{B}(L) \triangleq \frac{B(L)\Upsilon^2}{b_1^2((1-\mu^2)b_0+\sigma^2)^2 - (b_0 q)^2(b_0+b_1-2\mu\sqrt{b_0 b_1}+\sigma^2)^2}. \tag{38}$$

So, the bound on the bit-error probability is

$$P_b \le \frac{\tilde{B}(L_{\min})}{n} \sum_{j=1}^{\infty} w(j) \prod_{k=1}^{L} \frac{1}{4\beta^2\Upsilon|x_k - \hat{x}_k|^2}. \tag{39}$$

Next, we specialize this bound to several cases.

A. Ideally Interleaved Rayleigh Channels

In this case, $q = 0$ and (39) simplifies to

$$P_b \le \frac{\tilde{B}(L_{\min})}{n} \sum_{j=1}^{\infty} w(j) \prod_{k=1}^{L} \frac{4(1+(1-\mu^2)\gamma_s)}{\mu^2\gamma_s|x_k - \hat{x}_k|^2}. \tag{40}$$

This is the familiar Chernoff bound, with an additional multiplying factor. For codes with $L_{\min} = 2$, this factor tightens the ordinary Chernoff bound by about 3.3 dB in terms of the signal-to-noise ratio γ_s. This result is similar to the one derived by Chan and Bateman [17].

B. Ideal Trellis-Coded Multilevel Phase-Shift Keying (TC-MPSK)

In this case, it is assumed that prior measurements provide perfect channel estimation for each symbol interval. Thus, the channel estimates $\hat{\alpha}_k = \alpha_k$, their variance $b_1 = b_0 = 0.5$, and the correlation coefficient $\mu = 1$. Then, β would be (36)

$$\beta = \frac{\overline{E}_s}{2N_0}. \tag{41}$$

Substituting these values in (A.9) and (38) results in the following:

$$P(\boldsymbol{x} \to \hat{\boldsymbol{x}}) < \tilde{B}(L) \prod_{k=1}^{L} \frac{1}{(1-q^2)\frac{\gamma_s}{4}|x_k - \hat{x_k}|^2} \tag{42}$$

which when substituted in (39) yields

$$P_b \le \frac{\tilde{B}(L_{\min})}{n} \sum_{j=1}^{\infty} w(j) \prod_{k=1}^{L} \frac{1}{(1-q^2)\frac{\gamma_s}{4}|x_k - \hat{x_k}|^2}. \tag{43}$$

In comparison to ideal interleaving, the maximum signal-to-noise ratio degradation due to nonideal interleaving will be

$$\Theta = 10\log(1-q^2) \tag{44}$$

where q is the correlation between adjacent channel gains. For example, when the product $N_d f_D T_s$ increases from 0.01 to 0.2 the loss decreases from 9 to 0.3 dB. We may conclude that $N_d f_D T_s \approx 0.2$ is practically equivalent to ideal interleaving.

C. TC-MDPSK

In this case, for any signaling period, the preceding signal provides the channel estimate. Hence, the variance of the channel estimate is given by $b_1 = b_0 + \sigma^2$ and, assuming an exponential autocovariance function, it follows that

$$\mu^2 = \frac{b_0 \exp -(4\pi f_D T_s)}{b_0 + 0.5\gamma_s^{-1}} = \frac{\zeta^2}{1+\gamma_s^{-1}} \tag{45}$$

where $\zeta = \exp -(2\pi f_D T_s)$. These values can be readily substituted in (36), (A.9), (38), and (39) to get the union upper bound on P_b. For ideal interleaving, $q = 0$, and this reduces to [12, 9.119]. Also, since $\zeta < 1$, P_b will not decrease to zero when the signal-to-noise ratio $\gamma_s \to \infty$, giving rise to an error floor.

D. TC-MPSK with a Pilot Tone

As an alternative to differential detection, the α_k's may be measured using techniques such as a pilot tone [9] or embedded pilot symbols [18]. Here, a reference pilot tone is transmitted alongside the data signal. Assuming ideal filtering at the receiver, it can be shown that pilot estimate of the true channel gain will be [9], [15]

$$\hat{\alpha}_k = \alpha_k + \varsigma_k \tag{46}$$

where ς_k is an additive noise term with a variance of $0.5(B_p T_s)(\frac{1+r}{r})\gamma_s^{-1}$, in which B_p is the bandwidth of the pilot-tone filter, r is the power ratio between the pilot

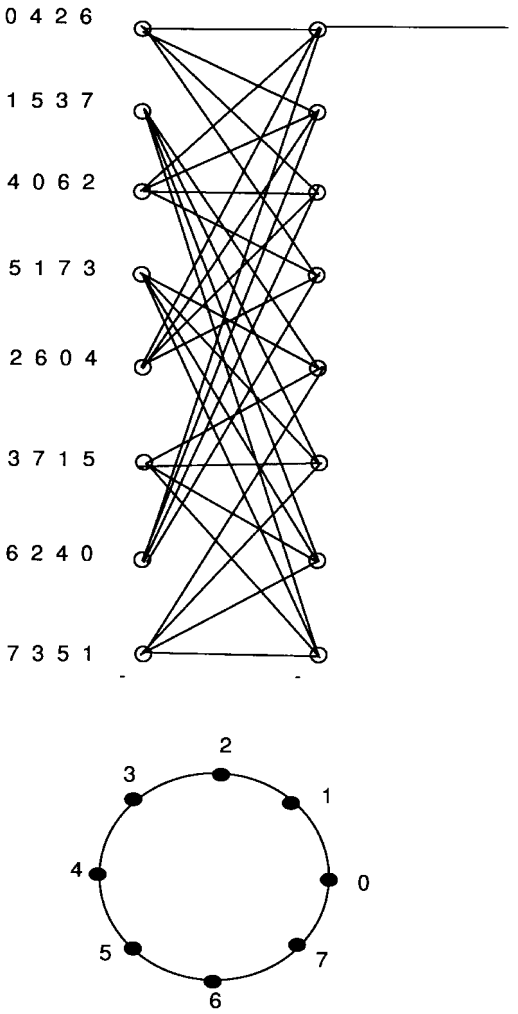

Fig. 2. Trellis diagram for eight-state 8PSK TCM scheme [19].

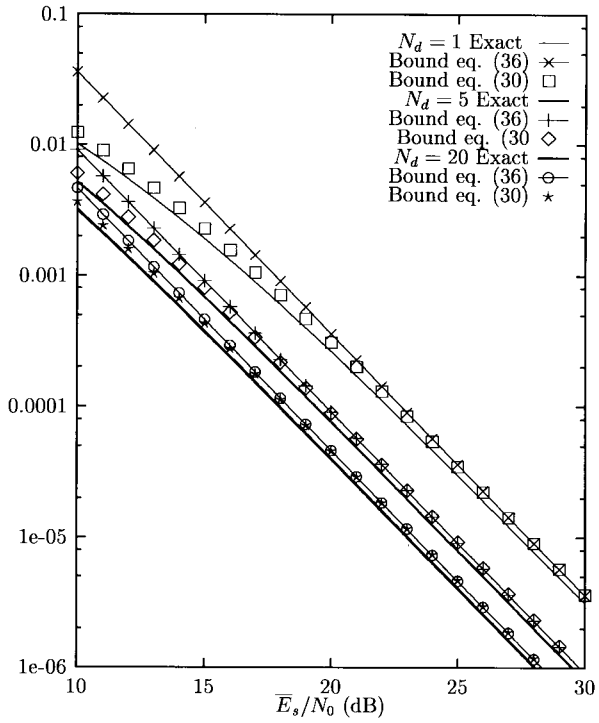

Fig. 3. Exact PEP [7] and the upper bound of an error event in a Rayleigh fading with ideal coherent detection. Exponential correlation with $f_D T_s = 0.01$.

signal and the data signal, and γ_s is the signal-to-noise ratio (including the power consumed by the pilot signal). As mentioned in [9], the bandwidth of the pilot-tone extraction filter should be sufficiently wide to allow for undistorted measurement of the fading process. Thus, $B_p = 2f_d$.

It can be readily shown that [15]

$$\text{var}\,(\hat{\alpha}_k) = b_1 = 0.5 + 0.5(B_p T_s)\left(\frac{1+r}{r}\right)\gamma_s^{-1}$$

$$|\mu|^2 = \frac{1}{1 + (B_p T_s)\left(\frac{1+r}{r}\right)\gamma_s^{-1}}. \tag{47}$$

Substituting these values in (36), (A.9), (38), and (39) results in the union bound.

V. Results

For several pertinent cases, the performance of the trellis code shown in Fig. 2 has been analyzed by using the error bounds developed earlier. To assess the accuracy of the error bounds, computer simulations have also been conducted. For simulation results, the interleaving span N_s was chosen to be 18 symbols.

To compute P_b given in (28), following [7], a set of error events have been picked from the modified error state diagram of this trellis code, as defined by Zehavi and Wolf [10]. Here, the set includes 14 dominant error events given in [7, Table 1] as well as 50 error events whose span is equal to four. These error events were found by searching through the error state diagram given in [19]. The details of the transfer function of this code can be found in [19].

Consider an error event of length two between the two codewords $\boldsymbol{x} = (1, 1, \cdots)$ and $\hat{\boldsymbol{x}} = (e^{j2\pi/4}, e^{j4\pi/4}, \cdots)$. For a Rayleigh fading channel with normalized Doppler 0.01, Fig. 3 depicts the exact PEP and the upper bounds (27) and (33) as functions of the signal-to-noise ratio $\overline{E}_s/N_0$ and the interleaving depth N_d. The exact PEP is computed by using the residue method [7]. It is clear that the upper bound (27) is extremely accurate while the accuracy of (33) increases as N_d increases. For Rician fading ($K = 5$ dB) with normalized Doppler 0.01, Fig. 4 shows the exact PEP and the upper bound (27) as functions of the signal-to-noise ratio $\overline{E}_s/N_0$ and the interleaving depth N_d. The exact PEP is computed by numerical integration of (14). It is seen that the upper bound (27) is very accurate for $P_b < 10^{-3}$. For instance, the difference between the two curves can be as small as 0.2 dB asymptotically. To put this in perspective, we note that the difference between the Chernoff upper bound, and the exact result for this particular error event can be 3.6 dB [9]. It is also noted that the accuracy of the bound increases as: 1) K decreases; 2) $\gamma_s \to \infty$; and 3) $N_d \to \infty$. This may be explained by noting that the bound ignores the phase function of the integrand in (14). For the same error event, the upper bound is plotted as a function of the interleaving depth N_d in Fig. 5 for two autocovariance functions: Bessel and exponential. For the exponential model, when the interleaving

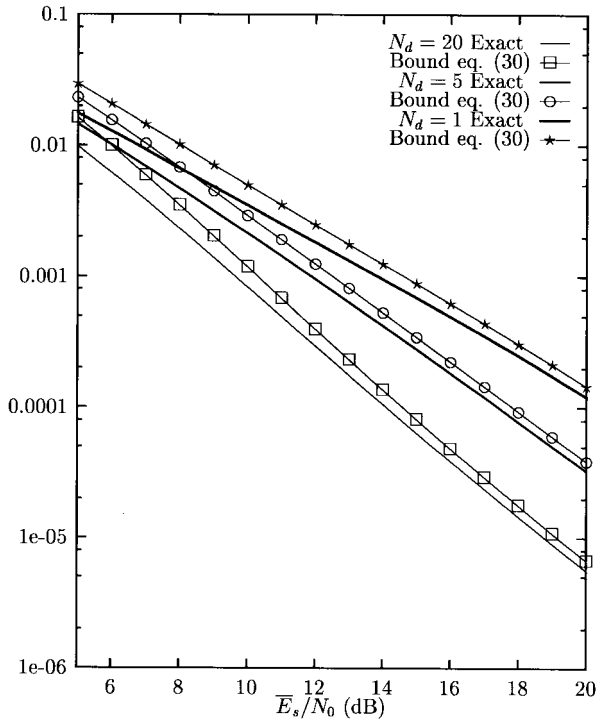

Fig. 4. Exact PEP and the upper bound of an error event in a Rician fading ($K = 5$ dB) with ideal coherent detection. Exponential correlation with $f_D T_s = 0.01$.

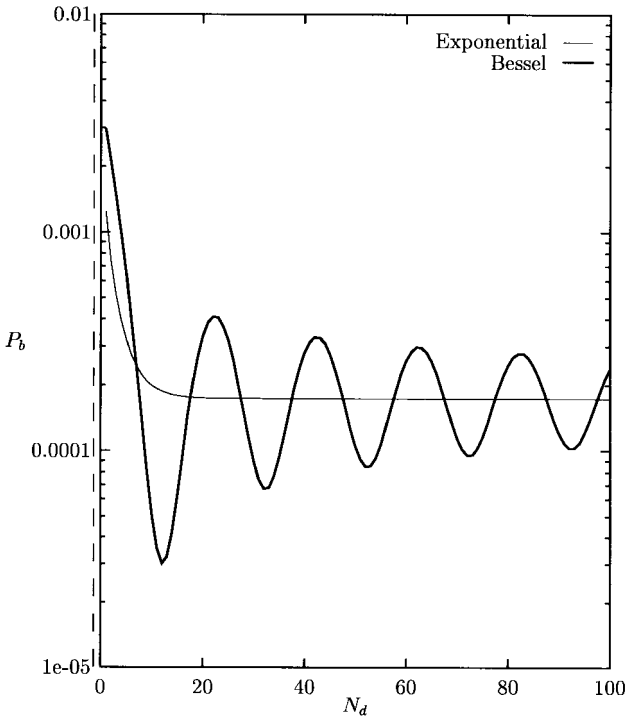

Fig. 5. Upper bound on the PEP versus the interleaving depth. Rician fading ($K = 5$ dB). $\overline{E_b}/N_0 = 12.0$ dB. Exponential correlation with $f_D T_s = 0.05$.

depth is such that $N_d f_D T_s \approx 0.5$, beyond which any increase of interleaving capacity does not reduce the error probability. As a matter of fact, $N_d f_D T_s \approx 0.2$ appears to be sufficient in this case. For the Bessel model, however, the error probability shows an oscillatory behavior; consequently, the optimum interleaving depth for a given Doppler is now $N_d f_D T_s \approx \theta_i$, where $J_0(\theta_i) = 0$, $i = 1, 2, \cdots$ and $J_0(x)$ is the zero-order Bessel function. These conclusions hold for most error events, and thus the overall bit-error probability would be affected in a similar manner.

For Rayleigh and Rician ($K = 5$ dB) fading with an exponential autocovariance function, the bound in (43), approximate P_b [see (28)], and simulation results are presented for the same trellis code in Figs. 6 and 7, respectively. Simulation results and the approximate P_b agree quite well even for the no-interleaving case. From Fig. 6, it can be seen that the bound (43) is quite accurate when interleaving depth and $\overline{E}_s/N_0$ are large. When no interleaving is employed, some of the simulation points are larger than the approximate P_b. This implies that more error events should be included in (28). Also, an interleaving depth of 20 symbols, resulting in a total interleaver capacity of 360 8PSK symbols, achieves almost 6-dB energy gain over no interleaving.

The performance of pilot-tone-aided detection is shown in Figs. 8 and 9. Once again, the approximate P_b is quite accurate for $N_d = 20$, implying that this amounts to almost ideal interleaving.

Fig. 10 shows the case of differential detection. Unfortunately, for an exponential covariance model, the quality of the channel estimates degrades rapidly even for small Doppler rates [see (45)]. This causes the bound (39) to be quite weak.

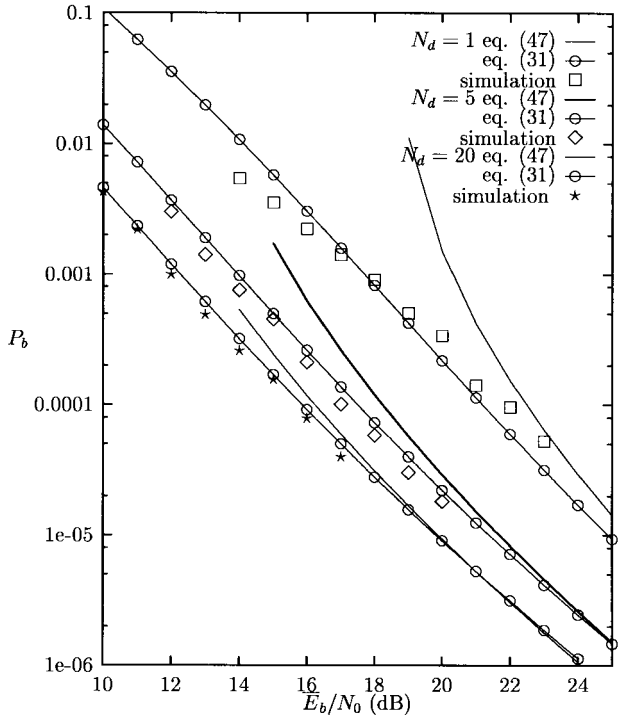

Fig. 6. Simulation, the approximate P_b, and the bound [43] of the eight-state trellis code. Rayleigh fading channel with ideal coherent detection. Exponential correlation with $f_D T_s = 0.01$.

VI. Conclusion

The error performance of TCM in correlated Rayleigh fading channels has been analyzed in [7] and [8]. However, for general Rician channels, no comparable results exist in the literature. In this paper, we have derived two general upper

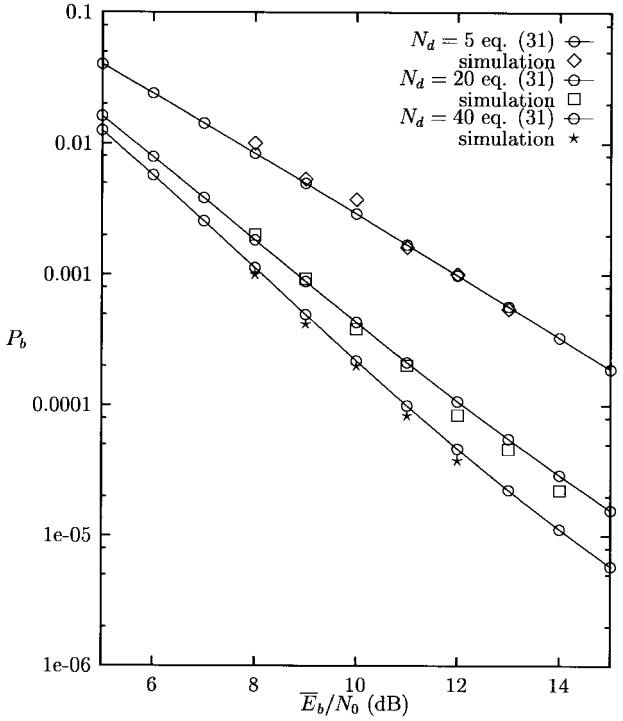

Fig. 7. Simulation and the approximate P_b of the eight-state trellis code. Rician fading ($K = 5$ dB) with ideal coherent detection. Exponential correlation with $f_D T_s = 0.01$.

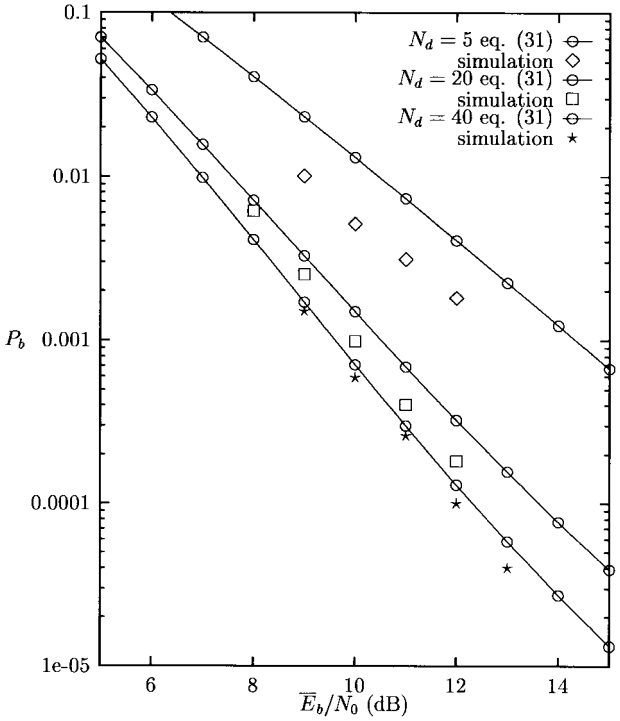

Fig. 9. Simulation and the approximate P_b of the eight-state trellis code. Rician fading ($K = 5$ dB) with pilot-tone coherent detection. Exponential correlation with $f_D T_s = 0.01$.

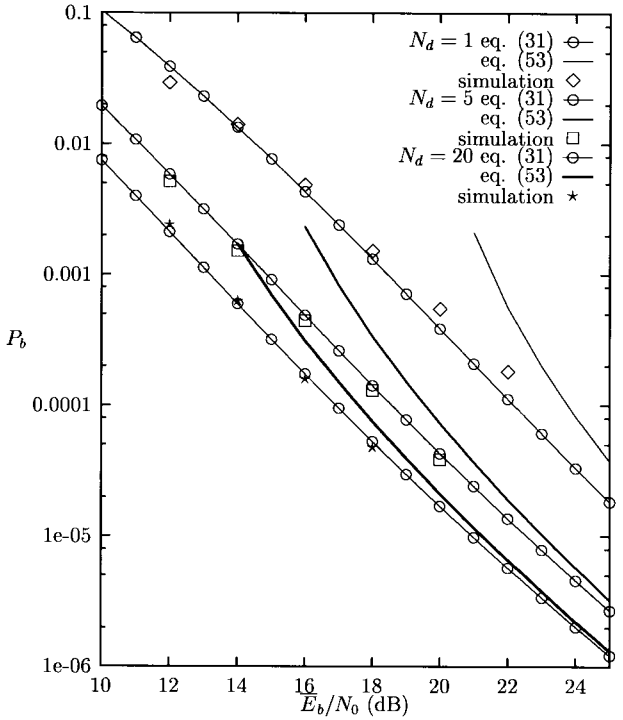

Fig. 8. Simulation results, the approximate P_b, and the bound [39] of the eight-state trellis code. Rayleigh fading with pilot-tone coherent detection. Exponential correlation with $f_D T_s = 0.01$.

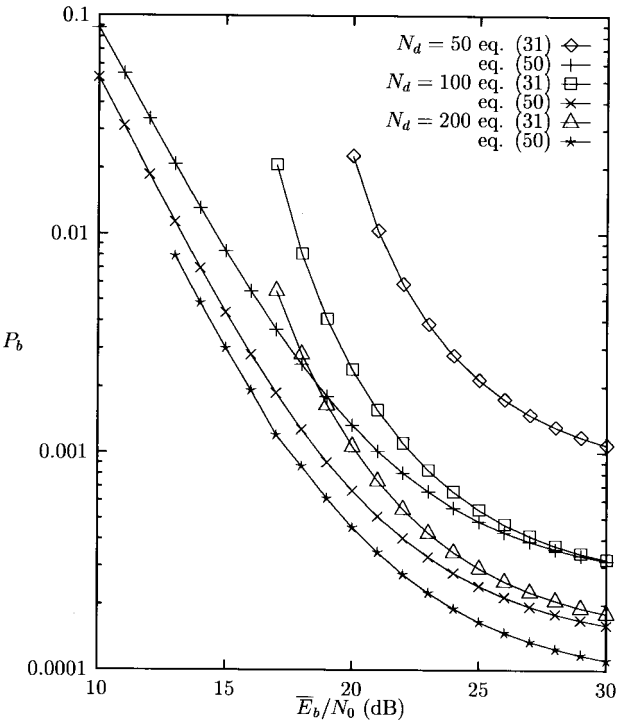

Fig. 10. Simulation and the approximate P_b of the eight-state trellis code. Rayleigh fading with differential detection. Exponential correlation with $f_D T_s = 0.001$.

bounds on the PEP, which are significantly more accurate than a Chernoff bound. These bounds can be used to provide an approximation to P_b by truncating the union bound to include a set of dominant error events. However, this approach may not be accurate when the correlation is high (due to insufficient interleaving capacity). The main problem then is that the tail of the union bound may even diverge. For Rayleigh fading channels with exponential correlation, a bound

on the PEP resembling that for memoryless channels has been derived. The bounds have been obtained assuming the pilot-tone concept, and hence can be modified to several useful cases. Comparison with simulation results shows that quite accurate estimates of P_b are obtainable with the use these bounds.

APPENDIX I
BOUND ON EIGENVALUES

Here, we would like to prove one case that supports the conjecture that the largest positive eigenvalue of $\boldsymbol{R}^*\boldsymbol{F}$ does not increase above the limit given by (35) as q changes from $q=0$ to $q>0$. We prove this only for error events of length two and ideal coherent detection.

Consider an error event of length two between $\boldsymbol{x}=(1,1)$ and $\hat{\boldsymbol{x}}=(x_1,x_2)$. In this case, the covariance matrix (11) is

$$\boldsymbol{R}=\begin{pmatrix} b_0 & b_0 & b_0q & b_0q \\ b_0 & b_0+\sigma^2 & b_0q & b_0q \\ b_0q & b_0q & b_0 & b_0 \\ b_0q & b_0q & b_0 & b_0+\sigma^2 \end{pmatrix}. \tag{A.1}$$

To find the eigenvalues of $\boldsymbol{R}^*\boldsymbol{F}$ the determinant of the matrix $\boldsymbol{R}^*\boldsymbol{F}-\phi I$ is equated to zero. After some manipulation, it can be shown that

$$\det\left(\boldsymbol{R}^*\boldsymbol{F}-\phi I\right)=D_1(\phi)D_2(\phi)-b_0^2q^2(\phi-\sigma^2)^2 \tag{A.2}$$

where

$$\begin{aligned} D_1(\phi) &\triangleq \phi^2+b_0|\delta_1|^2\phi-b_0|\delta_1|^2\sigma^2 \\ D_2(\phi) &\triangleq \phi^2+b_0|\delta_2|^2\phi-b_0|\delta_2|^2\sigma^2 \end{aligned} \tag{A.3}$$

$\delta_1=x_1-1$ and $\delta_2=x_2-1$. Denote by ϕ_{1+} and ϕ_{2+} the two positive roots of $D_1(\phi)=0$ and $D_2(\phi)=0$. From (35), $\max(\phi_{1+},\phi_{2+})<\sigma^2$. Let ϕ_+ denote the maximum positive root of (A2), which satisfies the condition

$$D_1(\phi_+)D_2(\phi_+)=b_0^2q^2(\phi_+-\sigma^2)^2. \tag{A.4}$$

By considering the graphs of these two curves (left and right sides of the equality sign), it can be shown that the solution ϕ_+ satisfies (35).

APPENDIX II
DETERMINANT OF $\boldsymbol{R}$

We wish to find the determinant of $\boldsymbol{R}$, denoted by D_L, as defined in (11). For this purpose, it is assumed that the positions of differing code symbols are adjacent in error events between codewords.

For $L=2$, we have the following matrix:

$$\boldsymbol{R}=\begin{pmatrix} R_0 & R_1 \\ R_1 & R_0 \end{pmatrix} \tag{A.5}$$

where R_0 is obtained from (11) with $x_k=1$ and R_1 is obtained from (12) with $\rho(|i-j|)=q$. The determinant of $\boldsymbol{R}$ is found to be

$$D_2=b_1^2((1-\mu^2)b_0+\sigma^2)-b_0^2q^2(2\mu\sqrt{b_0b_1}-b_0-b_1-\sigma^2)^2. \tag{A.6}$$

Considering $L=3$, we have the following matrix:

$$\boldsymbol{R}=\begin{pmatrix} R_0 & R_1 & qR_1 \\ R_1 & R_0 & R_1 \\ qR_1 & R_1 & R_0 \end{pmatrix} \tag{A.7}$$

which can be manipulated to find its determinant as

$$D_3\approx\Upsilon D_2 \tag{A.8}$$

where

$$\begin{aligned} \Upsilon=&(b_1-b_0q^2)(b_0+b_1+\sigma^2-2\mu\sqrt{b_0b_1}) \\ &-(b_1^2-2\mu b_1\sqrt{b_0b_1}+\mu^2b_0b_1). \end{aligned} \tag{A.9}$$

In (A.8), we use the approximation sign because two terms of the expansion have been neglected. The neglected terms tend to zero as $q\to 0$ and $\sigma^2\to 0$.

Continuing in this manner, we get

$$D_L\approx\Upsilon^{L-2}D_2. \tag{A.10}$$

ACKNOWLEDGMENT

The authors wish to thank the anonymous reviewers for their useful suggestions.

REFERENCES

[1] J. N. Pierce and S. Stein, "Multiple diversity with nonindependent fading," *Proc. IRE*, vol. 48, pp. 196–211, Oct. 1960.
[2] F. Gagnon and D. Haccoun, "Bounds on the error performance of coding for nonindependent Rician fading channels," *IEEE Trans. Commun.*, vol. 40, pp. 351–360, Feb. 1992.
[3] A. N. Trofimov, "Convolutional codes for channels with fading," *Prob. Inform. Trans.*, vol. 27, pp. 155–165, Oct. 1991.
[4] G. Kaplan and S. Shamai (Shitz), "Achievable performance over the correlated Rician channel," *IEEE Trans. Commun.*, vol. 42, pp. 2967–2978, Nov. 1994.
[5] ——, "Error performance over the uninterleaved correlated Rician fading channel," in *Proc. Int. Symp. Information Theory*, San Antonio, TX, Jan. 1993, pp. 105–105.
[6] D. L. Noneaker, "The effect of finite interleaving depth on the performance of convolutional codes in rician-fading channels," in *Proc. Int. Symp. Information Theory*, 1994.
[7] P. Ho and D. Fung, "Error performance of interleaved trellis-coded PSK modulations in correlated Rayleigh fading channels," *IEEE Trans. Commun.*, vol. 40, pp. 1800–1809, Dec. 1992.
[8] C. Schlegel, "Trellis coded modulation on time-selective fading channels," *IEEE Trans. Commun.*, vol. 42, nos. 2/3/4, pp. 1617–1627, 1994.
[9] J. K. Cavers and P. Ho, "Analysis of the error performance of trellis coded modulations in Rayleigh fading channels," *IEEE Trans. Commun.*, vol. 40, pp. 74–83, Jan. 1992.
[10] E. Zehavi and J. K. Wolf, "On the performance of trellis codes," *IEEE Trans. Inform. Theory.*, vol. IT-33, pp. 196–202, Mar. 1987.
[11] D. Divsalar and M. K. Simon, "Trellis-coded modulation for 4800 to 9600 bps transmission over a fading satellite channel," *IEEE J. Select. Areas. Commun.*, vol. SAC-5, pp. 162-175, Feb. 1987.
[12] E. Biglieri, P. J. McLane, M. K. Simon, and D. Divsalar, *Introduction to Trellis-Coded Modulation with Applications*. New York: McMillan, 1991.
[13] J. K. Cavers, "On the validity of the slow and moderate fading models for matched filter detection of Rayleigh fading signals," *Can. J. Elect. Comput. Eng.*, vol. 17, pp. 183–189, Oct. 1992.
[14] M. Schwartz, W. R. Bennett, and S. Stein, *Communication Systems and Techniques*. New York: McGraw-Hill, 1966.
[15] C. Tellambura, Q. Wang, and V. K. Bhargava, "A performance analysis of trellis-coded modulation schemes over Rician fading channels," *IEEE Trans. Veh. Technol.*, vol. 42, pp. 490–501, Nov. 1993.
[16] I. N. Sneddon, *Special Functions in Mathematical Physics and Chemistry*. London, U.K.: Longman, 1980.
[17] K. Chan and A. Bateman, "The performance of reference-based M-ary PSK with trellis coded modulation in Rayleigh fading," *IEEE Trans. Veh. Technol.*, vol. 41, pp. 190–198, May 1992.

[18] J. K. Cavers, "An analysis of pilot symbol assisted modulation for Rayleigh fading channels," *IEEE Trans. Veh. Technol.*, vol. 40, pp. 686–693, Nov. 1991.
[19] R. G. McKay, E. Biglieri, and P. J. McLane, "Error bounds for trellis-coded MPSK on a fading mobile satellite channel," *IEEE Trans. Commun.*, vol. 39, pp. 1750–1761, Dec. 1991.

C. Tellambura received the B.Sc. degree in electronics and communications engineering from the University of Moratuwa, Sri-Lanka, in 1986, the M.Sc. degree in electronics from the King's College, London, U.K., in 1988, and the Ph.D. degree in electrical engineering from the University of Victoria, Victoria, B.C., Canada, in 1993.

He was with the University of Moratuwa from 1986 to 1987 and from 1988 to 1989 and with the University of Victoria from 1993 to 1994. From 1995 to 1996, he was a Research Fellow with the Department of Electronic and Electrical Engineering, University of Bradford, U.K. He is now with the Department of Digital Systems, Monash University, Clayton, Victoria, Australia. His current research interests include indoor wireless communications.

Vijay K. Bhargava (S'70–M'74–SM'82–F'92), for a photograph and biography, see this issue, p. 83.